NUCL SCI TECH (2020) 31:33
https://doi.org/10.1007/s41365-020-0751-7

Feasibility of an innovative long-life molten chloride-cooled reactor

Ming Lin[1,2] · Mao-Song Cheng[1] · Zhi-Min Dai[1]

Received: 28 October 2019 / Revised: 16 February 2020 / Accepted: 17 February 2020 / Published online: 14 March 2020

Abstract Molten salt-cooled reactor is one of the six Gen-IV reactors with promising characteristics including safety, reliability, proliferation resistance, physical protection, economics, and sustainability. In this paper, a small innovative molten chloride-cooled fast reactor (MCCFR) with 30-year core and a target 120-MWt thermal power was presented. For its feasible study, neutronics, thermal-hydraulics, and radiation damage analysis were performed. The key design properties including kinetics parameters, reactivity swing, reactivity feedback coefficients, maximum accumulated displacement per atom (DPA) of reactor pressure vessel (RPV) and fuel cladding, and maximum coolant, cladding, and fuel temperatures were evaluated. The results showed the MCCFR could operate without refueling for 30 years with overall negative reactivity feedback coefficients up the end of its life. During its 30-year life, the excess reactivity was well managed by constantly pulling out the control rods. The maximum accumulated DPA on RPV and fuel cladding were 8.92 dpa and 197.03 dpa, respectively, which are both below the design limits. Similarly, the maximum coolant, cladding and fuel center temperatures were all below the design limits during its entire lifetime. According to these results, the MCCFR core design with long life is feasible.

Keywords Molten salt-cooled reactor · Neutronics · Radiation damage · Thermal-hydraulics

1 Introduction

As one of the six highest potential reactor types proposed by the Generation IV International Forum, molten salt-cooled fast reactor has drawn much attention due to its strong inherent safety and favorable neutronic economy. Molten chloride salt is a preferred coolant in nuclear reactor systems, which displays superiority in its higher thermodynamic efficiency, higher volumetric heat capacity, high boiling point, harder neutron spectrum, and excellent natural circulation performance [1, 2]. The potential benefits of small modular reactors without on-site refueling include lower construction costs, lower investment costs and risks, possibly greater or easier nonproliferation, and enhanced safety [3]. With these, a 120 MWt small modular molten chloride-cooled fast reactor (MCCFR) with 30-year life without on-site refueling is proposed.

The application of liquid salt on the reactor technology is derived from the 2.5 MW aircraft reactor experiment (ARE) and molten salt reactor (MSR) project developed at Oak Ridge National Laboratory (ORNL) [4]. The liquid salt-cooled reactor attracted researchers again until the 2000s, when several kinds of liquid salt fuel and liquid salt-cooled reactors were investigated, such as 2-MW and 373-MW molten salt reactors [5, 6], advanced high-temperature reactor (AHTR) [7], small modular advanced

This work was supported by Strategic Pilot Science and Technology Project of Chinese Academy of Sciences (No. XD20191031).

✉ Mao-Song Cheng
mscheng@sinap.ac.cn

Ming Lin
linming@sinap.ac.cn

[1] Shanghai Institute of Applied Physics, Chinese Academy of Sciences, Jiading Campus, Shanghai 201800, China

[2] University of Chinese Academy of Sciences, Beijing 100049, China

high-temperature reactor (SmAHTR) [8], and ordered-pebble-bed fluoride-salt-cooled high-temperature experimental reactor [9]. A flexible conversion ratio for a fast reactor using molten chloride salt as coolant was proposed due to its low moderating capacity at the Massachusetts Institute of Technology (MIT) [10]. Later, a compact liquid chloride salt-cooled fast reactor (SPARK-LS) was also suggested in Xi'an Jiaotong University [11]. Compared to liquid fluoride salt, chloride salts are preferable in realizing a high conversion ratio and achieving a long core lifetime for small modular reactors.

MCCFR is designed for local small grids operating for a long period without refueling. To achieve its design goals, there are several design requirements proposed for the MCCFR core design:

(1) For the safety operation of the reactor, small reactivity swing and negative overall reactivity feedback coefficients are required during the core lifetime.
(2) One of the important life-limiting factors of a reactor is the state of its structural materials. Structural materials, such as the reactor pressure vessel (RPV) and fuel cladding, are continuously damaged and irradiated by neutrons particularly fast neutrons, gamma ray, and other particles from fission reactions. The integrated measure of their damage is represented by the displacement per atom (DPA), which is the number of times each atom is displaced from its lattice site. DPA could be applied for the characterization of varying mechanical properties and corrosion resistance, which guides the material endurance. The safe operation of MCCFR should ensure the integrity of RPV and fuel cladding over the core lifetime [12].
(3) Molten salt-cooled reactors have higher operating temperatures than traditional pressurized water reactors. Hence, for the purpose of meeting certain economic and safety considerations, a set of design limits should be implemented in the thermal-hydraulics design of the MCCFR core. These design limits are focused on the coolant, cladding, and fuel temperatures.

This paper focuses on the conceptual design, neutronic characteristics analysis, radiation damage, fuel swelling analysis, and preliminary thermal-hydraulic performance evaluation of the MCCFR core. The main goal of this paper is to perform a feasibility study of an innovative MCCFR. Firstly, MCCFR, which can approach long cycle and high burnup, is described. Secondly, its steady-state neutronics and depletion behavior are analyzed. Thirdly, the maximum accumulated DPA of RPV and fuel cladding materials are assessed by their design criteria, followed by performing a fuel swelling analysis. Finally, its main thermal-hydraulic parameters are calculated and evaluated using a sub-channel analysis code. The results achieved in this paper will provide reliable evidence for the ultra-long life of the MCCFR core.

2 MCCFR core description

2.1 Design objective and constraints

For the safe operation of MCCFR, the main key design constraints listed in Table 1 are proposed.

(1) The reactor is designed for 30 years without refueling.
(2) The shutdown margin of the reactor must be maintained as larger than 1000 pcm [13].
(3) The reactivity coefficient of the reactor and other various reactivity coefficients including fuel Doppler coefficient, coolant temperature coefficient, void coefficient reactivity, and radial and axial expansion coefficient should be negative throughout the core lifetime.
(4) In order to maintain its safety, the control rods are inserted in the core to introduce sufficient negative reactivity to compensate for the built-in (positive) reactivity at the beginning of core life (BOL). During the core burnup, the excess reactivity should be managed by constantly pulling out the control rods.
(5) The maximum DPA of the RPV should below 200 dpa [14].
(6) The maximum DPA of SiC/SiC_f should be less than 200 dpa [15]. For a traveling wave reactor, the peak irradiation dose may be as high as 500 dpa.
(7) A temperature of 450 °C is set as the minimum coolant temperature of NaCl–KCl–$MgCl_2$ to provide sufficient margin to prevent freezing. The maximum

Table 1 Design limits of MCCFR

Parameters	Design criteria
Design lifetime (years)	30
Temperature reactivity coefficient	Negative
Core shutdown margin	> 1000 pcm
DPA limit of Hastelloy-N	< 200
DPA limit of SiC/SiC_f	< 200
Coolant temperature (°C)	$450 < T < 1400$
SiC/SiC_f cladding temperature (°C)	< 900
(Pu–U)N fuel centerline temperature (°C)	< 3035

coolant temperature is set as its boiling temperature of 1400 °C.

(8) The fuel centerline temperature should not exceed the maximum temperature of 3035 °C at the hottest fuel pin [16].

(9) For the purpose of ensuring the integrity of the fuel pins, the maximum cladding temperature should be less than 900 °C [17].

2.2 Parameters of the MCCFR core

MCCFR is designed to operate at a 120-MW thermal power without refueling for 30 years [18]. The schematic of its primary cooling system is depicted in Fig. 1a. The primary coolant of molten chloride salt is driven by natural circulation during a nominal steady-state operation and after shutdown. Molten chloride salt has large thermal expansion coefficient, which makes natural circulation highly possible. The heat generated in the reactor core is transported to the heat exchanger by the circulating molten salt. The cooled molten salt leaving the heat exchanger flows down through the downcomer to the lower plenum before reentering the core.

The configuration of the MCCFR core is shown in Fig. 1b, and its design and operating parameters are listed in Table 2. The active core length and diameter are designed as 125 cm and 134 cm, respectively. Figure 1b, c shows the fuel rod configuration: 2.62 cm in diameter, 0.02 cm gas gap, 0.2 cm thickness cladding, and 3.10 cm fuel rod pitch, thereby resulting in a pitch-to-diameter ratio of 1.18. The core contains five zones with different fuel enrichment. Two central low enrichment zones corresponding to 1.2 and 2.6 Pu/HM% enrichment and three enrichment zones corresponding to 12.8, 14.1, and 15.4 Pu/HM % enrichment are designed to lower the power peak and the burnup reactivity swing. The core consists of a single cassette/assembly composed of 1566 rods clustered in groups. From the innermost to outermost area from zone 1–5, the numbers of rods are 84, 144, 402, 360, and 566, respectively. Two sets of control rods are provided to

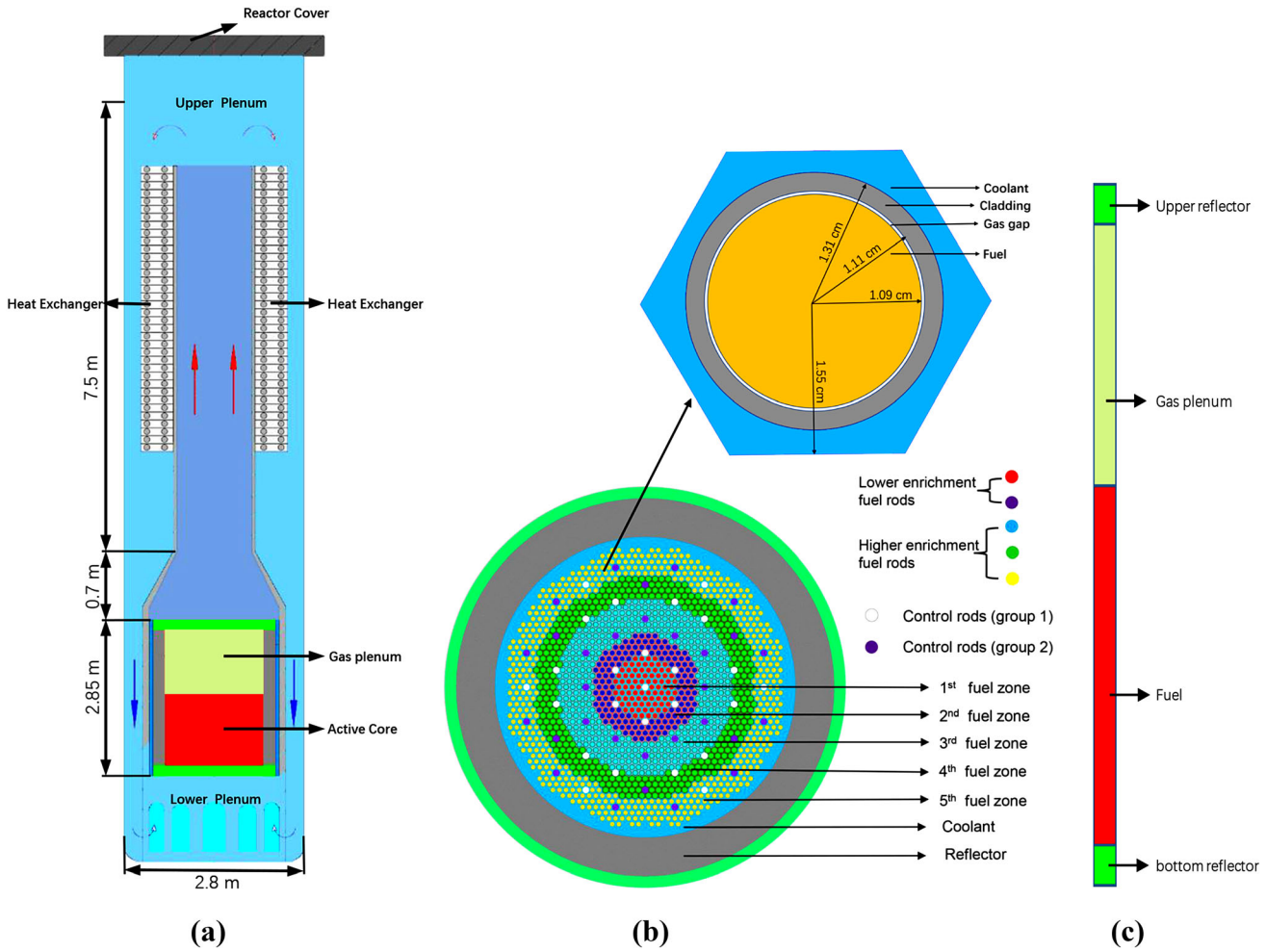

Fig. 1 (Color online) Schematic of MCCFR: of primary cooling system (**a**), core configuration (**b**), and fuel rod (**c**)

Table 2 Parameters of the MCCFR core

Parameters	Value
Geometric parameters	
Power (MWt)	120
Fuel	(Pu–U)N fuel
Coolant	NaCl–KCl–$MgCl_2$ (30–20–50%) mol%
Cladding	SiC/SiC_f
Structure material	Hastelloy-N
Reflector material	Titanium
Number of fuel rod from inner to outer core	84/144/402/360/566
Number of control rods	Two sets control system (25/30)
Enrichment (Pu/HM%)	1.2/2.6/12.8/14.1/15.4
Discharge burnup (MWd/kg HM)	131
Fuel/gap/cladding outer diameter (cm)	2.18/2.22/2.62
Fuel pin/control rod diameter (cm)	2.62
Pitch-to-diameter ratio	1.18
Wire diameter (cm)	0.34
Wire axial pitch (cm)	25
Active core height/diameter (cm)	125/134
Inlet operating characteristics	
Inlet temperature (°C)	500
Inlet coolant flow rate (kg/s)	4180.5
Inlet coolant velocity (m/s)	4.38
Average heat flux (W/cm^2)	74.9

control the reactivity and to shut down the reactor. The inlet temperature of the coolant and inlet mass flow is set to 500 °C and 4180.5 kg/s, respectively.

In the design of the MCCFR core, (Pu–U)N fuel is selected due to its high density, high thermal conductivity, high melting temperature, low swelling, thermal stability, and low fission gas release [19]. The isotopic vectors of plutonium listed in Table 3 are obtained from the spent fuel discharged from LWRs with 50 MWd/kgHM burnup and 5-year cooling [20]. This plutonium is then blended with natural uranium (0.7 wt% ^{235}U) then enriched in N^{15} to form (Pu–U)N fuel. The compositions of (Pu–U)N fuel in five fuel regions are shown in Table 4.

The ternary NaCl–KCl–$MgCl_2$ (30–20–50%) salt is selected as the most suitable coolant salt for high power density fast reactor applications. The salt was also applied to design a flexible conversion ratio for the fast reactor of Petroski [21] in MIT. Hastelloy-N (INOR-8) is recommended as the structural material in MCCFR design. In order to reduce the coolant void reactivity, titanium was used as the reflector material on account of its low density, good corrosion resistance, and large strength-to-density ratio. In fission nuclear reactors, the fuel cladding is an extremely crucial security barrier. In recent years, silicon has been widely used in reactors [22] with SiC/SiC_f cladding considered as the priority candidate materials for Gen-IV reactors. In the current design, SiC/SiC_f is used as the cladding material of the MCCFR. The cladding liner is used to prevent possible incompatibility with nitride fuel [17].

Table 3 Isotopic vectors of plutonium

Isotope	wt%
^{238}PU	1.6
^{239}PU	58.2
^{240}PU	23.5
^{241}PU	11.2
^{242}PU	5.5

3 Analysis tools and methodology

In the neutronics analysis of the core design, SCALE6.1/CSAS6 was used to evaluate *k*-effective (k_{eff}) and SCALE6.1/TRITON was applied for burnup calculation. Criticality Safety Analysis Sequence with KENO-VI (CSAS6) was developed to provide cross-sectional processing followed by the calculation of the neutron multiplication factor for systems modeled using KENO-VI [23]. TRITON computer code is a multipurpose SCALE control module for transport, depletion, uncertainty, and sensitivity analysis [24].

Table 4 Compositions of (Pu–U)N fuel

Isotope	First fuel region	Second fuel region	Third fuel region	Fourth fuel region	Fifth fuel region
^{238}Pu (wt%)	0.0203	0.0418	0.2052	0.2267	0.2470
^{239}Pu (wt%)	0.7376	1.5187	7.4634	8.2444	8.9821
^{240}Pu (wt%)	0.2978	0.6132	3.0135	3.3290	3.6268
^{241}Pu (wt%)	0.1420	0.2923	1.4362	1.5865	1.7285
^{242}Pu (wt%)	0.0697	0.1435	0.7053	0.7791	0.8488
^{15}N (wt%)	5.9000	5.9000	5.9000	5.9000	5.9000
^{235}U (wt%)	0.7113	0.7016	0.6280	0.6184	0.6092
^{238}U (wt%)	92.1213	90.7889	80.6483	79.3160	78.0577
Density (g/cm^3)	14.3000	14.3000	14.3100	14.3100	14.3100

In order to achieve self-sustaining and stable operation for 30 years, the reactivity control code coupling CASA6 and TRITON modules in SCALE6.1 code package was built to manage the excess reactivity during burnup. The flowchart of the code is illustrated in Fig. 2. At the beginning, the code will guess a reasonable position of the control rods and evaluate k_{eff} through CASA6. Linear interpolation method was applied to obtain the position of control rods until k_{eff} achieves the critical condition. Subsequently, depletion calculations are executed to note the control rods depletion and fuel density change, which should be taken into consideration in the code. The next cycle will read the standard composition specifications as part of the input to provide the fuel state at the beginning of the next operational cycle. This cycle will repeat the aforementioned processes until the cycle is stopped.

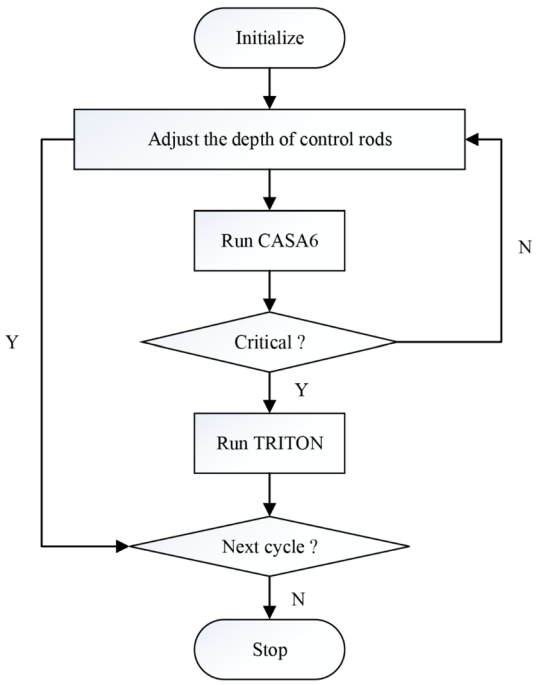

Fig. 2 Flowchart of reactivity control code

Radiation damage is usually quantified by DPA. In order to perform the calculations, a fine discretization in energy was implemented in the DPA cross section and the rate of DPA was calculated from the following formula [12]:

$$R_{\text{DPA}} = \int_{E_{\text{g}}}^{E_{\text{G}}} \Phi(E_i)\delta_{\text{dis}}(E_i)\mathrm{d}E_i \cong \sum_{i=1}^{N} \phi_i \cdot \delta_{\text{dis}}^{i}, \quad (1)$$

where E_{G} is the maximum energy of the incident particle, E_{g} is the minimum energy of the incident particle, $\delta_{\text{dis}}(E_i)$ is the energy-dependent displacement cross section, and $\Phi(E_i)$ is the energy-dependent particle flux per unit energy. ϕ_i and δ_{dis}^{i} are the microscopic cross section and flux in the i group, respectively. The accumulated DPA is then computed by

$$\text{DPA}^{n+1} = \text{DPA}^{n} + \Delta T \sum_{i=1}^{N} \delta_{\text{dis}}^{i} \cdot \phi_i \quad (2)$$

For the thermal-hydraulic analysis of the MCCFR design, the core consists of only a single cassette/assembly composed of 1566 rods clustered in groups; so, sub-channel analysis method should be employed in the core. In recent years, a series of codes [25, 26] was developed by the Shanghai Institute of Applied Physics for molten salt reactor. The sub-channel analysis code (TSUB) is developed and validated for thermal-hydraulic analysis of MCCFR [18]. In TSUB, a single-phase model is used due to the high boiling point ($\sim$ 1400 °C) of molten chloride salt, which is considered as an incompressible liquid. TSUB code is applied for evaluating the thermal-hydraulic design parameters of MCCFR in terms of the coolant, cladding and fuel temperature distributions in its core.

4 Neutronics analysis

MCCFR reactor with 120-MW thermal power can operate for 30 effective full power years (EFPY) without refueling. Figure 3a shows the normalized neutron spectra of the MCCFR core. Figure 3b shows the variations of k_{eff} over time. The initial k_{eff} is 1.0525, and the burnup reactivity swing is 4988.1 pcm. k_{eff} declined rapidly at BOL. After around 10 years, there are more ^{238}U, which would be converted to ^{239}Pu, thereby causing the slow decrease of the reactivity until it reached zero. The key core k_{eff}, reactivity coefficients, and kinetic parameters of MCCFR at BOL and end of core life (EOL) are shown in Table 5. The reactor has negative overall reactivity feedback coefficients including the fuel, coolant, core radial, and axial expansions reactivity coefficients, and coolant void reactivity during the lifetime. The fuel Doppler coefficient further decreased at EOL due to the slightly softened neutron spectrum caused by the accumulation of fission products. The coolant void reactivity in the full core is negative during the core lifetime. The radial power factors at BOL and EOL are shown in Fig. 4. The peak radial power factor is 1.328 and 1.325 at BOL and EOL, respectively. At BOL, the power densities of the inner two fuel zones are significantly small and the outer three fuel zones had more contributions to the core power. At EOL, the maximum power zone moved toward the core center owing to the fuel loading pattern strategy. At a higher burnup, the outer fuel zones is depleted and the Pu quality deteriorated while the inner fuel zones accumulated enough fissile material, resulting in larger radial power factors of the inner fuel zones than those in the outer ones.

As shown in Fig. 1b, two groups of control rods, each composed of 25 control rods, are provided for the independence and redundancy of the scram. Group 1 is applied for both normal control of the reactor (start-up, reactivity control during core lifetime, and power regulation) and shutdown. Group 2 is applied for emergency shutdown. The control rods are made of B_4C with a B-10 concentration of 94%. When both control rods groups are completely inserted, k_{eff} is 0.90945 (hot condition) and 0.91447 (cold condition). Therefore, these two control systems could meet the shutdown margin (1000 pcm) in the MCCFR core. This will ensure the safety of the reactor during accidents. Table 6 shows the control rod worth of group 1 and 2 rods under different operating conditions. At EOL, the control rod worth of group 1 was significantly reduced at EOL. When group 1 control rods are inserted in the reactor, the Boron concentration decreased due to neutron irradiation during the core lifetime. This would significantly reduce the control rod worth of group 1. Although group 2 control rods are not inserted into the core, its control rod value is also reduced due to the neutron flux change at EOL. In the reactor, group 1 control rods are withdrawn from the core to compensate excess reactivity. Figure 5a shows the position of the group 1 control rods every burnup cycle during operation. All control rods are then extracted after 30 years. Figure 5b shows good results of the k_{eff} swing between 0.9995 and 1.0005, which could ensure safe operation of the reactor during its lifetime. The burnup cycle is 50 days in BOL and 100 days after 40 cycles. Hence, the line is compact in the first 6 years. At EOL, the fluctuation range of the reactivity is significantly reduced. This effective reactivity control strategy could

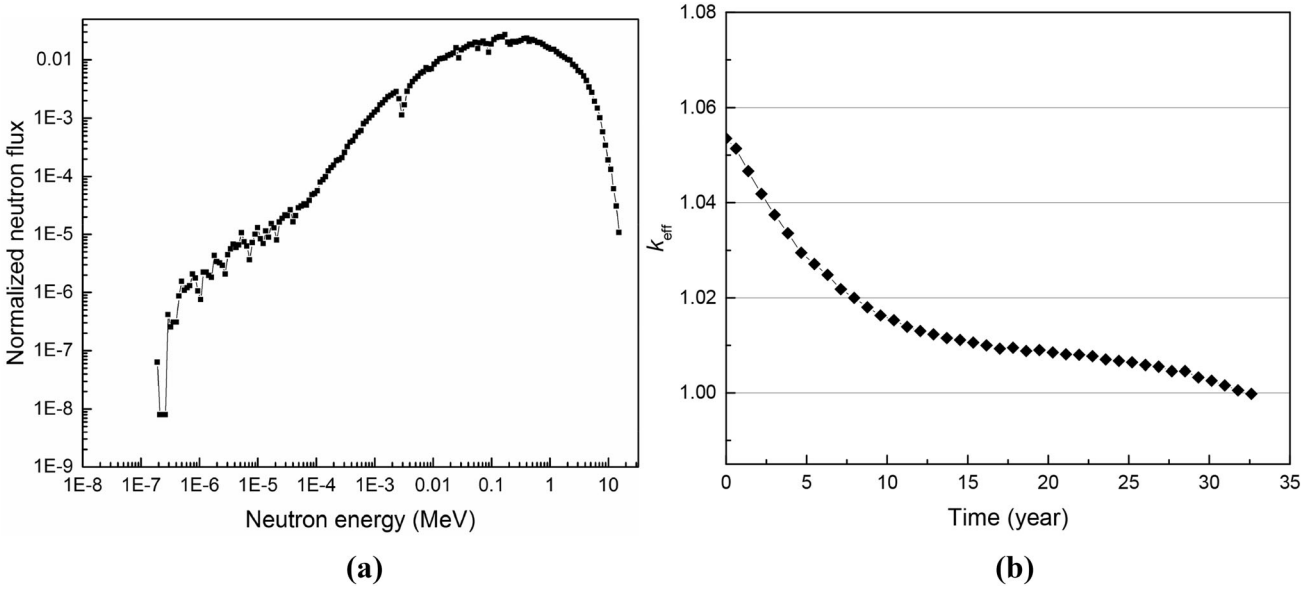

Fig. 3 Normalized neutron spectra of MCCFR core (**a**) and k_{eff} variations during its lifetime (**b**)

Table 5 Reactivity feedback coefficients and kinetics parameters at BOL and EOL

Design parameters	Beginning of core life (BOL)	End of core life (EOL)
k-effective	1.0525	1.0080
Effective delayed neutron fraction (pcm)	431	414
Prompt neutron lifetime (ns)	291.5	243.8
Fuel Doppler coefficient (pcm/K)	− 0.645	− 0.723
Coolant temperature coefficient (pcm/K)	− 0.201	− 0.135
Axial/radial expansion coefficient (pcm/K)	− 0.191/− 0.682	− 0.186/− 0.654
Coolant void reactivity (CVR) in the full core (pcm)	− 1233.300	− 921.600

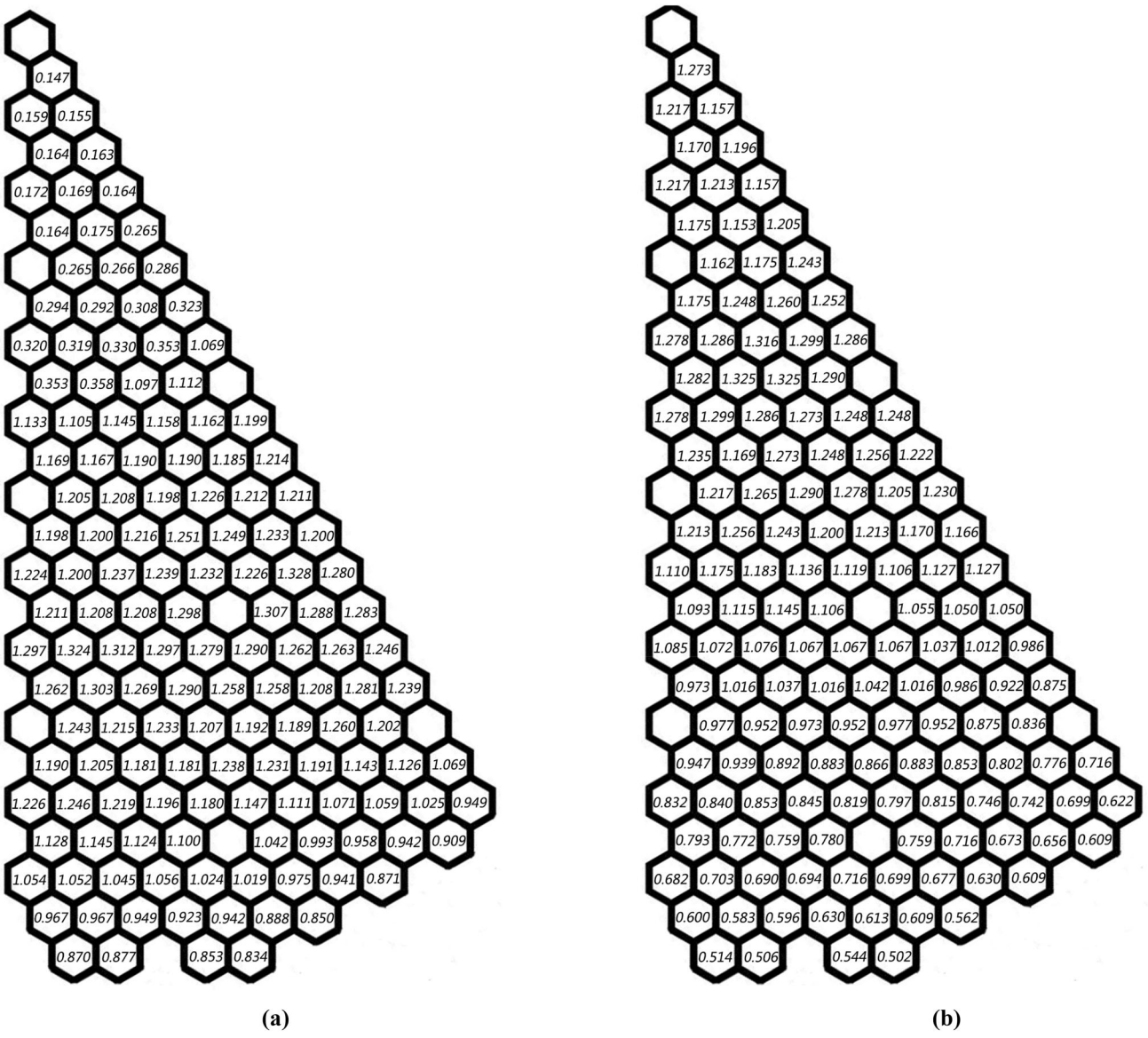

Fig. 4 Radial power distribution at BOL (**a**) and EOL (**b**)

achieve self-sustaining and stable operation for 30 years without on-site refueling.

The fuel compositions in the core at BOL and EOL are shown in Table 7. After 30 EFPY of depletion, 4710.6 and

Table 6 Control rod worth of group 1 and 2 rods

Control rods group	Group 1 control rod worth (pcm)	Group 2 control rod worth (pcm)	Total control rod worth (pcm)
BOL (hot/cold)	6166.9/6355.4	7699.7/7916.8	13,866.6/14,272.1
EOL	5455.3	7244.1	12,699.4

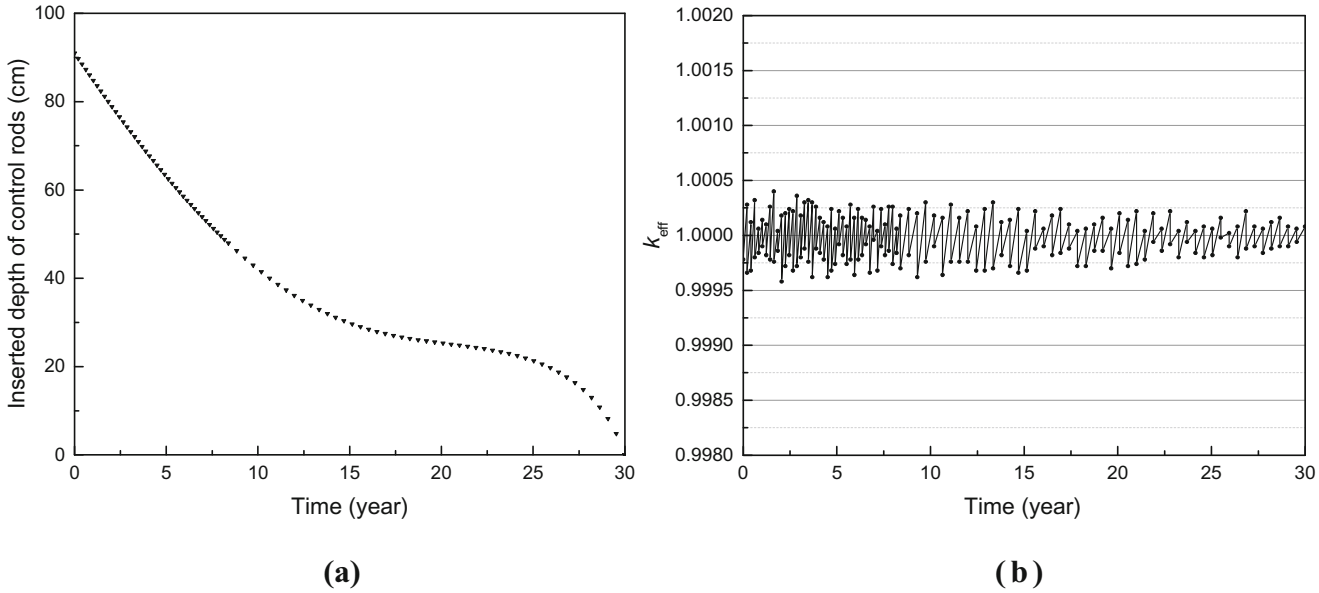

Fig. 5 The inserted depth of control rods (**a**) and the variation of k_{eff} with control rods moving during core lifetime (**b**)

Table 7 Fuel compositions in the core at BOL and EOL

Isotope	First fuel region (g)	Second fuel region (g)	Third fuel region (g)	Fourth fuel region (g)	Fifth fuel region (g)	Total (g)
^{235}U (BOL)	416.5	738.2	1801.0	1568.0	2106.0	6629.7
^{235}U (EOL)	85.8	163.8	436.6	455.1	777.7	1919.0
^{238}U (BOL)	53,940.0	95,520.0	231,000.0	200,900.0	269,500.0	850,860.0
^{238}U (EOL)	43,840.0	78,100.0	188,900.0	168,300.0	234,700.0	713,840.0
^{237}Np (BOL)	0.0	0.0	0.0	0.0	0.0	0.0
^{237}Np (EOL)	36.1	67.1	219.3	193.8	272.1	788.5
^{238}Pu (BOL)	12.9	47.6	645.3	631.3	939.1	2276.2
^{238}Pu (EOL)	28.6	76.4	704.6	671.3	1040.0	2520.9
^{239}Pu (BOL)	468.4	1735.0	23,470.0	22,960.0	34,160.0	82,793.4
^{239}Pu (EOL)	4615.0	8212.0	24,110.0	21,710.0	31,090.0	89,737.0
^{240}Pu (BOL)	189.1	700.6	9477.0	9270.0	13,790.0	33,426.7
^{240}Pu (EOL)	957.1	1864.0	10,410.0	9679.0	14,800.0	37,710.1
^{241}Pu (BOL)	90.1	333.9	4517.0	4418.0	6573.0	15,932.0
^{241}Pu (EOL)	78.3	161.2	1102.0	999.9	1531.0	3872.4
^{242}Pu (BOL)	44.2	163.9	2218.0	2169.0	3228.0	7823.1
^{242}Pu (EOL)	46.9	157.3	1948.0	1925.0	3022.0	7099.2
^{241}Am (BOL)	0.0	0.0	0.0	0.0	0.0	0.0
^{241}Am (EOL)	45.5	130.2	1416.0	1502.0	2605.0	5698.0

137,020.0 g of ^{235}U and ^{238}U were consumed, respectively, and ^{239}Pu was bred from ^{238}U with a net product of 6943.6 g. The mass of ^{239}Pu increased in the first, second, and third fuel regions while that of the fourth and fifth fuel region decreased. Moreover, the mass of ^{238}Pu and ^{240}Pu increased while that of ^{241}Pu and ^{242}Pu decreased. The reason for the significant decrease of the fissionable isotope ^{241}Pu is its lower half-life than other plutonium isotopes. The mass of ^{242}Pu converted by ^{241}Pu is less than its consumption, causing the decline of its own mass. The mass of minor actinides such as ^{237}Np and ^{241}Am all significantly increased due to the relatively higher plutonium enrichment in MCCFR.

5 RPV and fuel cladding radiation damage and fuel swelling analysis

5.1 Radiation damage of RPV and fuel cladding

The calculation formulas of the rate of DPA and accumulated DPA are shown in Sect. 3. The neutron flux distribution of the MCCFR core is calculated and generated by SCALE6.1/CSAS6. A total of 86 energy groups of DPA cross section for Hastelloy-N is shown in Fig. 6a [27]. Chang et al. [28] obtained the displacement damage cross section of SiC/SiC$_f$ shown in Fig. 6b by applying Norgett Robinson–Torrens model.

In order to evaluate the DPA of the reactor pressure vessel (RPV), the calculation model can be simplified as Fig. 7 with respect to θ = 30° plane according to symmetry of the core. Figure 8a, b shows the rate of DPA (R_{DPA}) on the inner surface of the RPV at BOL and EOL, respectively. The maximum R_{DPA} is 9.368e−09 and 9.491e−09 dpa/s at BOL and EOL, respectively. At EOL, the neutron flux in the core is higher than in BOL, causing a larger maximum R_{DPA} at BOL. The results indicate that the maximum irradiation dose at EOL for the RPV is about 8.92 dpa, which is far from the 200 dpa limit.

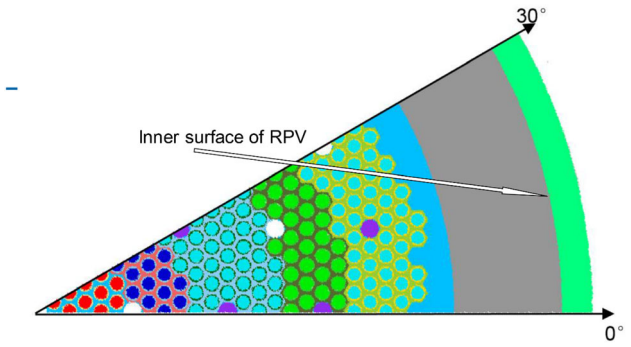

Fig. 7 (Color online) Simplified calculation model

Figure 9 illustrates R_{DPA} distribution of the SiC/SiC$_f$ cladding at BOL, middle of life (MOL), and EOL. The maximum R_{DPA} shifted inward toward the centerline due to the shift of the maximum neutron flux toward the core center during the lifetime. The maximum values of R_{DPA} are 2.209e−07, 2.162e−07, and 2.395e−07 dpa/s at BOL, MOL, and EOL, respectively. The maximum irradiation dose at EOL for SiC/SiC$_f$ cladding in the MCCFR core is about 197.03 dpa, which is smaller than the 200 dpa limit.

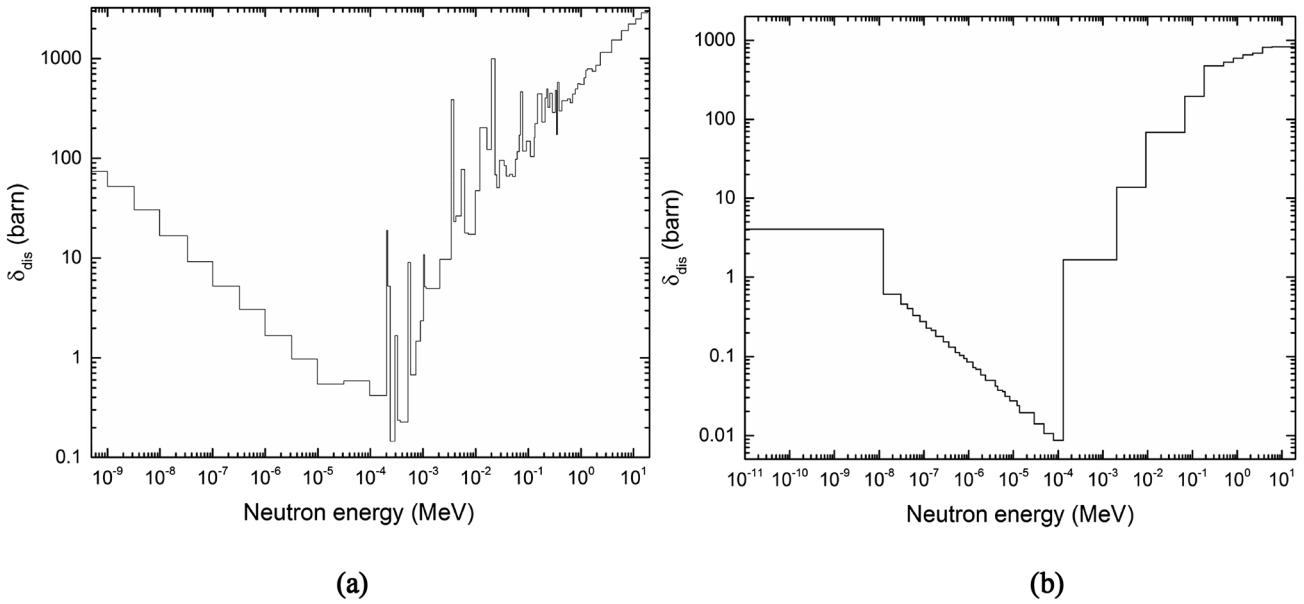

Fig. 6 DPA cross section of Hastelloy-N (**a**) and SiC/SiC$_f$ (**b**)

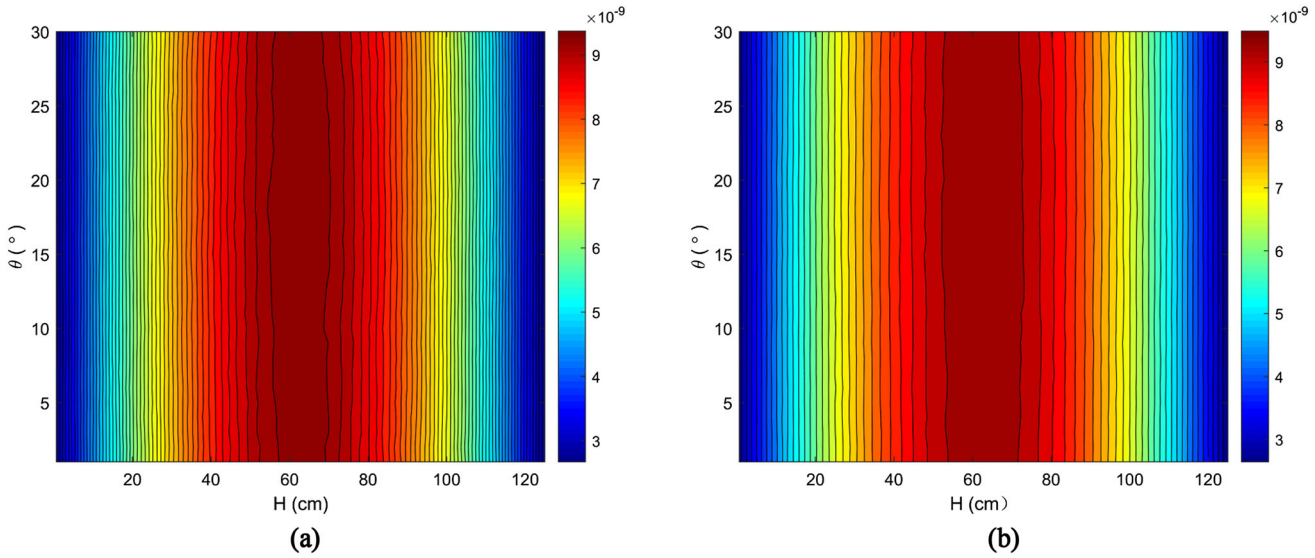

Fig. 8 (Color online) R_{DPA} in term of Z and Theta on the inner surface of the RPV at BOL (**a**) and EOL (**b**)

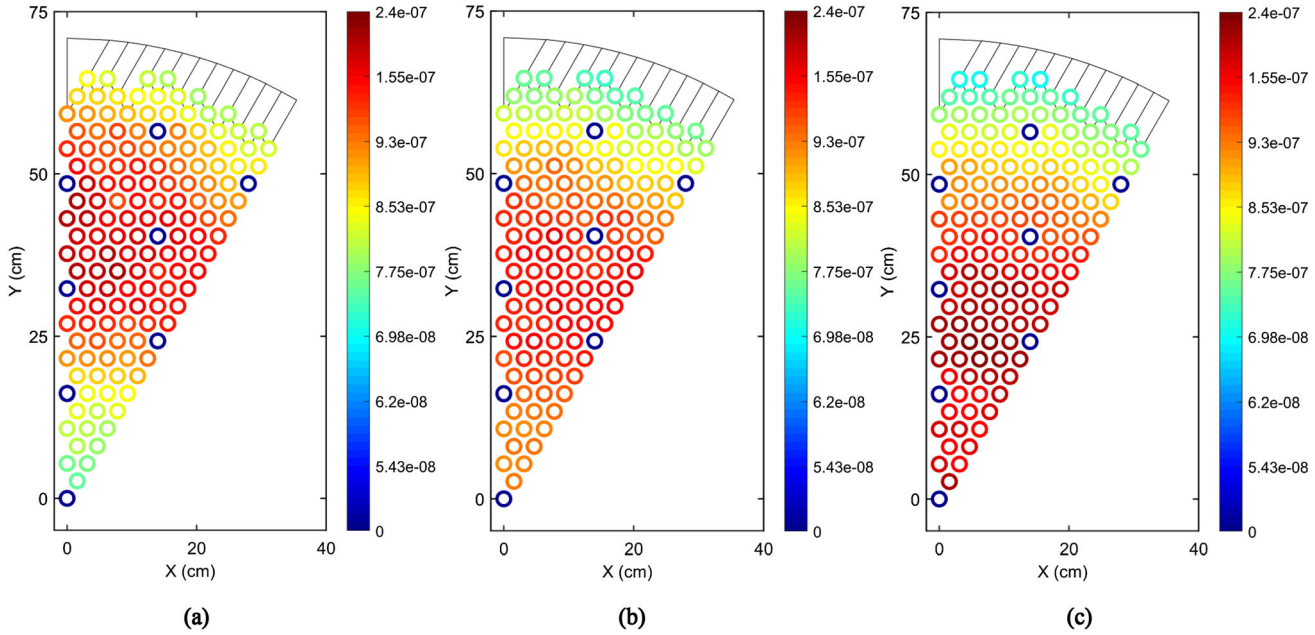

Fig. 9 (Color online) R_{DPA} distribution of SiC/SiC_f cladding at BOL (**a**), MOL (**b**), and EOL (**c**)

5.2 Fuel swelling

The peak fuel centerline temperature of MCCFR calculated by TSUB is 1363.4 °C at BOL. For low temperatures (fuel centerline temperature < 1400 °C), more realistic average values of the total volumetric fuel swelling rate were recommended with about 0.8% $\Delta V/V$ (fuel volume change at per % burnup [29].

The burnup is then calculated using the formula:

$$\text{BU}\ (\%\text{FIMA}) = (ND_{\text{BOL}} - ND_{\text{EOL}})/ND_{\text{BOL}}, \quad (3)$$

where ND_{BOL} is the density of heavy metal atoms at BOL and ND_{EOL} is the density of heavy metal atoms at EOL. The value of BU calculated by SCALE6.1/TRITON is 10.8% FIMA and $\Delta V/V$ is 8.64% at EOL. To accommodate fuel swelling and fission gas release, the ratio of the gas plenum (included gas gap) to the fuel volume is designed as high as 82%. Nitride fuels have been successfully developed and irradiated to a high burnup of up to 20% FIMA [30].

6 Thermal-hydraulics analysis

The power distribution of the MCCFR core used as the input data of the TSUB code calculated and generated by SCALE6.1/CSAS6. Gnielinski, Cheng–Todreas, and Rogers–Rosehart correlations are utilized for heat transfer, pressure drop, and turbulent mixing models, respectively [18]. For the thermal-hydraulic design and analysis of the MCCFR core using TSUB code, it is necessary to first define the numbering of the rods and sub-channels. Due to symmetry of the core, 1/12 symmetrical cross section of the core is modeled and 18 axial nodes are adopted for the MCCFR. Figure 10 indicates the numbering of the sub-channels starting from the center of the core. There are 262 sub-channels including 250 interiors and 12 edge sub-channels at 151 rods. In Fig. 10, the green sub-channels (sc3, sc20, sc77, sc102, and sc164) correspond to two lower enrichment zones (1st and 2nd) and three higher enrichment zones (3rd, 4th and 5th). To compare within different enrichment zones, five sub-channels are selected for comparison in this study.

Figure 11 (Color online) shows the temperature distribution of molten chloride salt coolant, fuel interior, and fuel cladding in the 1/12 symmetrical core at BOL. The temperature ranges from 500 to 1400 °C in the core. The temperatures of the fuel rods are much higher than that of the coolant. The maximum temperature is obtained between the axial location of $Z = 60$ cm and $Z = 70$ cm.

Considering the influence of temperature on the corrosion behavior of the cladding material, a detailed analysis of the local temperatures of each sub-channel and fuel rod is critical. The power density and neutron flux of the MCCFR core continuously changed during the core lifetime. With this, the following analyses are carried out at the BOL, MOL, and EOL.

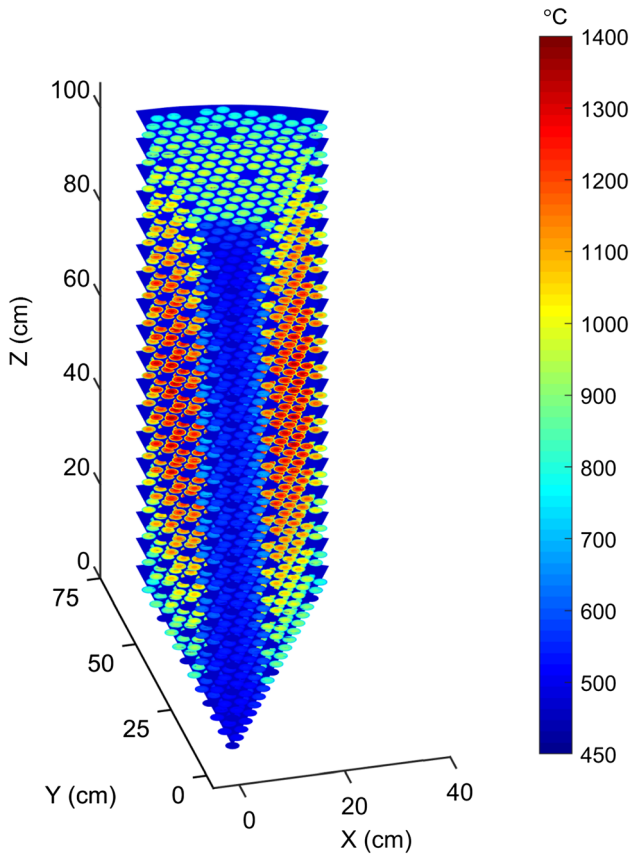

Fig. 11 (Color online) The temperature distribution in the 1/12 symmetrical core

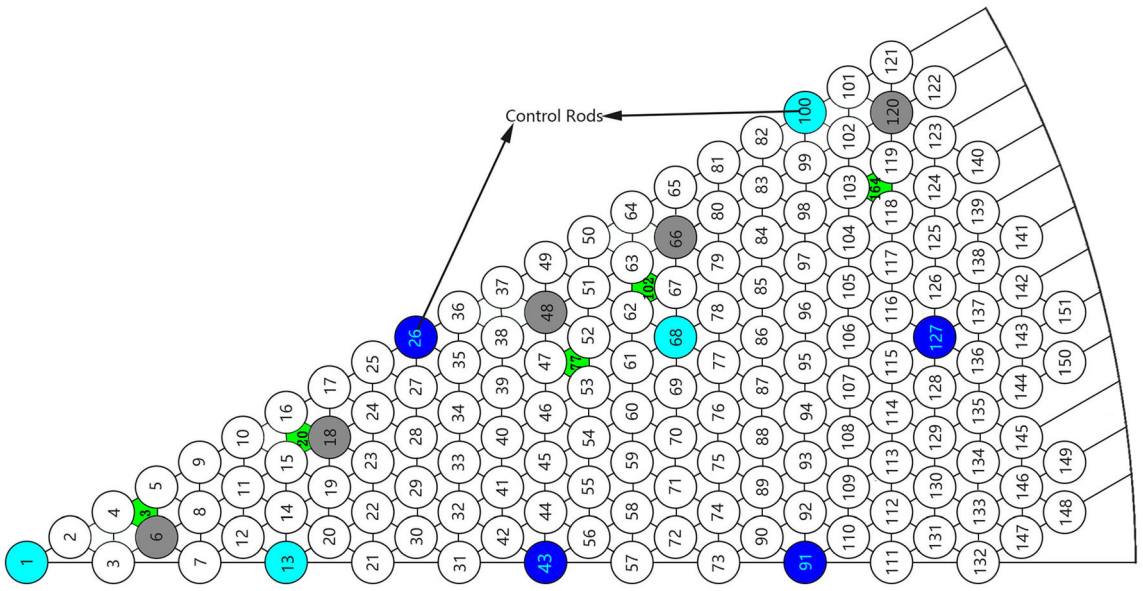

Fig. 10 (Color online) Numbering scheme of 142 sub-channels

Figure 12 illustrates the distribution of the coolant temperatures of sc3, sc20, sc77, sc102, and sc164 in the five fuel zones over the active heights at BOL, MOL, and EOL. At BOL, due to lower enrichment in the two central zones (1st and 2nd) and large neutron leakage in the core boundary, sc102 corresponding to the fourth fuel zone was recorded as the hottest channel. As the operation proceeds, ^{238}U in the two central lower enrichment zones is converted to ^{239}Pu during burnup. The peak power/burnup location gradually shifted toward the center, temporarily resulting in the highest temperatures of different pins. At MOL, sc77 became the hottest channel. At EOL, the increase in the channel temperature gradually shifted into the inner zone of the reactor. The maximum coolant temperatures are as high as 551.8 °C, 550.0 °C, and 557.3 °C at BOL, MOL, and EOL, respectively. The inlet temperature of 500 °C is the minimum coolant temperature, which is higher than the temperature limit of 450 °C. Moreover, the maximum coolant temperature of the core in different periods is significantly lower than the coolant boiling temperature design limit of 1400 °C.

Figures 13 and 14 describe the temperature distributions at the hottest layer of the claddings and fuel rods at BOL, MOL, and EOL. The radial temperature distribution

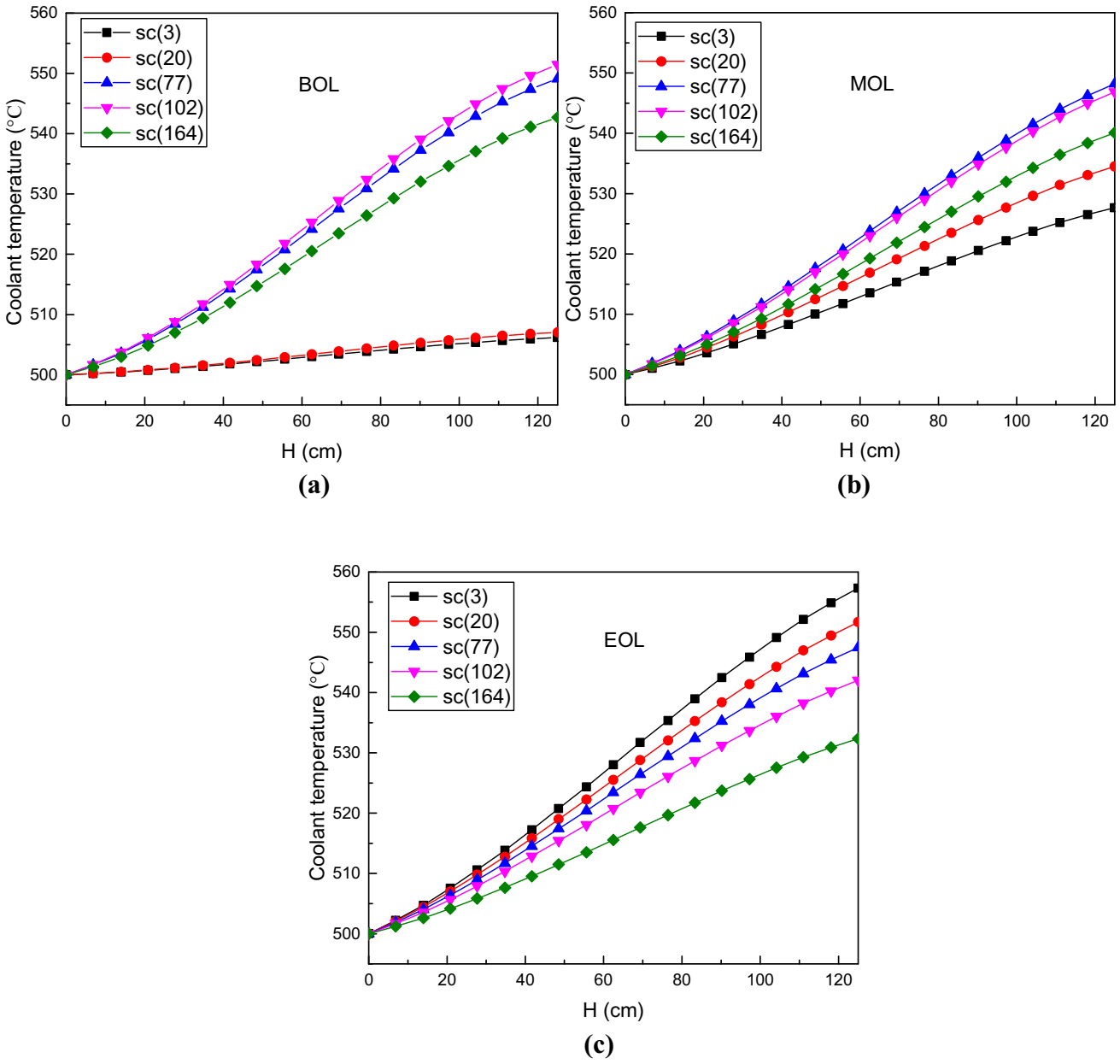

Fig. 12 (Color online) Distribution of coolant outlet temperature in 1/12 symmetrical core at BOL (**a**), MOL (**b**), and EOL (**c**)

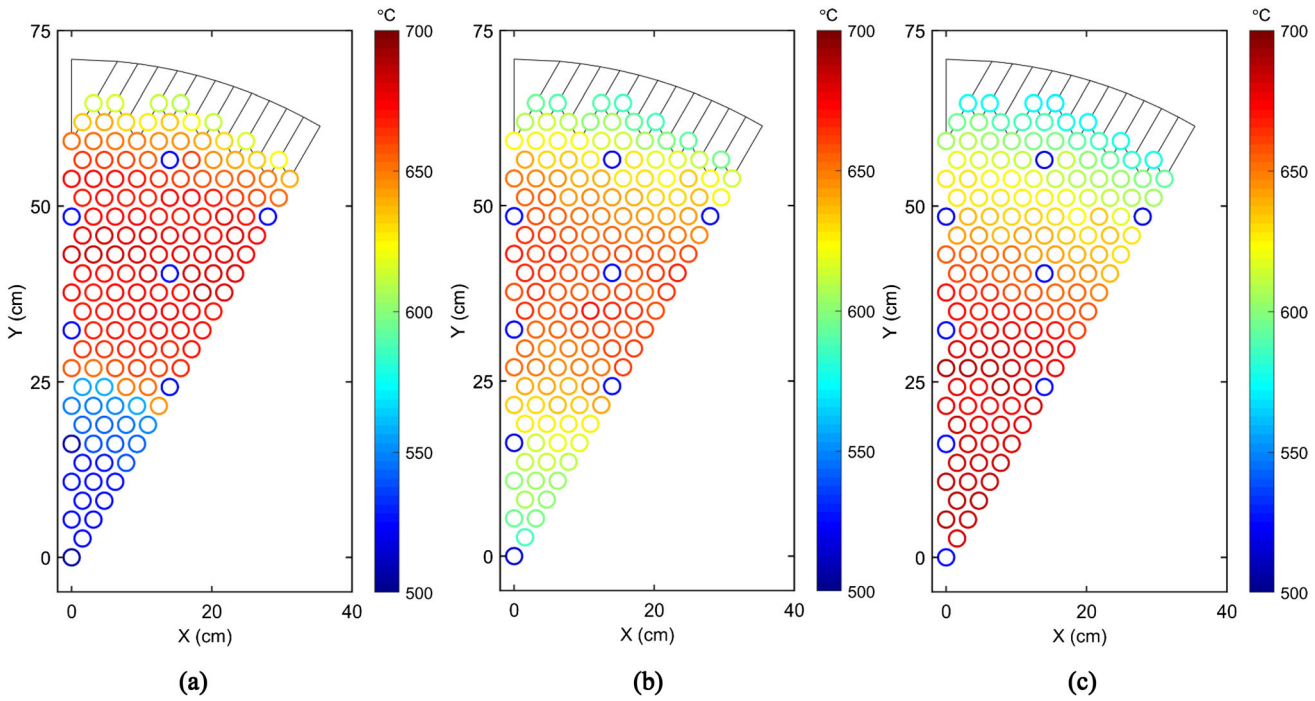

Fig. 13 (Color online) Distribution of cladding outer temperature at the hottest layer at BOL (**a**), MOL (**b**), and EOL (**c**)

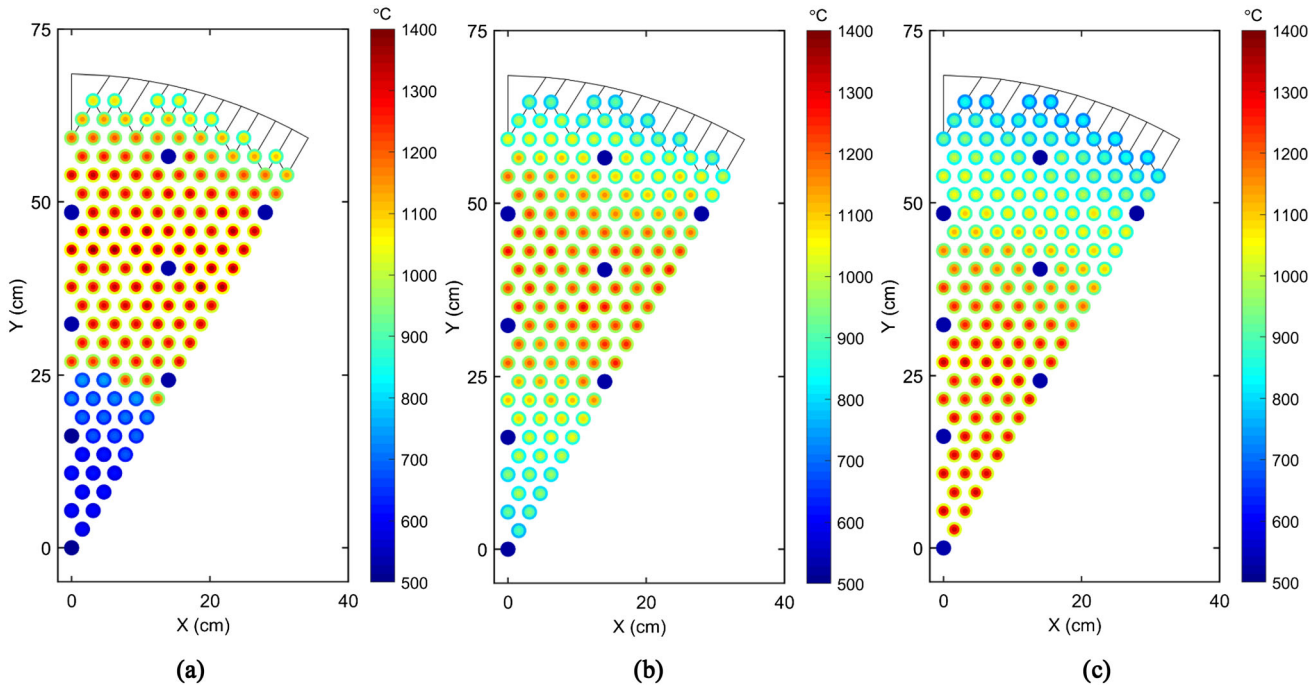

Fig. 14 (Color online) Distribution of fuel temperature at the hottest layer at BOL (**a**), MOL (**b**), and EOL (**c**)

gradient is similar to that of the coolant temperature, where the hottest temperatures of the claddings and fuel rods shifted toward the centerline. Figure 15a, b shows the hottest cladding outer and fuel centerline temperatures, respectively, along the axial direction during BOL, MOL and EOL. The peak cladding outer temperature reached as high as 681.2 °C in rod66, 668.3 °C in rod53, and 674.5 °C in rod6 at BOL, MOL, and EOL, respectively. The peak fuel centerline temperature is as high as 1363.4 °C at BOL, 1298.8 °C at MOL, and 1318.5 °C at EOL. The peak cladding is far below the cladding temperature limit of

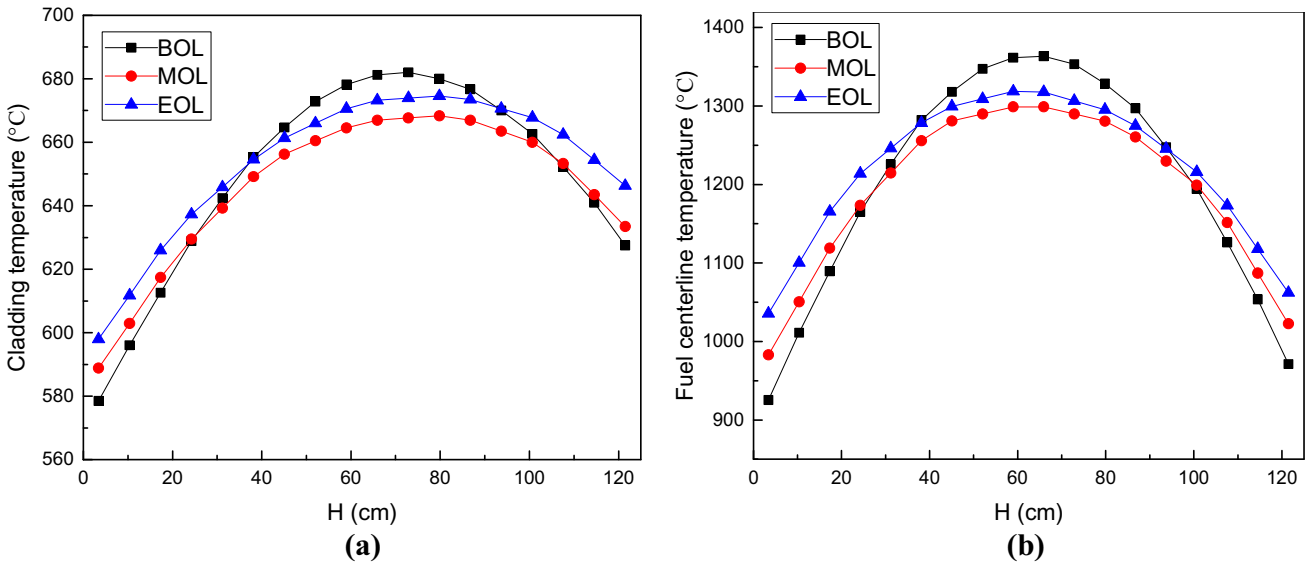

Fig. 15 (Color online) Distribution of cladding temperature and fuel centerline temperature along the axial direction of the core in five representative sub-channels

900 °C, and the fuel centerline temperature is below the melting temperature of 3035 °C during different periods.

7 Conclusion

In this study, an innovative conceptual design of a small molten chloride-cooled fast reactor with 30-year life without on-site refueling is proposed. To evaluate the feasibility of its core design, neutronics, thermal-hydraulics, radiation damage, and fuel swelling analysis were performed using analysis tools, including SCALE6.1, reactivity control, and TSUB codes. The results are as follow:

(1) The initial k_{eff} is 1.0525, and burnup reactivity swing is 4988 pcm during 30 EFPY. The reactivity coefficients provided sufficient negative feedback. Two control systems were also implemented to provide sufficient shutdown margins. This ensured the safety of the reactor should accidents occur. The effective reactivity control strategy could achieve self-sustaining and stable operation for 30 years without on-site refueling.

(2) The maximum irradiation dose at EOL for the RPV and fuel cladding is 8.92 and 197.03 dpa, respectively, which are both less than the design limit of 200 dpa. At EOL, the total fuel volume expanded by 8.64%.

(3) The maximum coolant temperature, cladding temperature, and fuel centerline temperature at BOL, MOL and EOL were all lower than the design limits.

Therefore, these confirm the feasibility of the preliminary conceptual design of the MCCFR core. For future studies, safety analysis could be performed to ensure the inherent safety feature of MCCFR.

References

1. J.J. Bulmer, Fused Salt Fast Breeder: Reactor Design and Feasibility Study. United States Atomic Energy Commission, Technical Information Service Extension, vol. 56 (1957), pp. 8–204
2. R. Petroski, H. Pavel, E.T. Neil, Thermal hydraulic design of a liquid salt-cooled flexible conversion ratio fast reactor. Nucl. Eng. Des. **239**(12), 2612–2625 (2009). https://doi.org/10.1016/j.nucengdes.2009.07.012
3. Status of Small Reactor Designs Without On-Site Refuelling (IAEA-TECDOC-1536, Vienna, 2007)
4. M.W. Rosenthal, P.R. Kasten, R.B. Briggs, Molten-salt reactors—history, status, and potential. Nucl. Technol. **8**, 107–117 (1970)
5. L. He, C.G. Yu, W. Guo et al., The temperature distribution of molten salt reactor under the outer salt layer blocked situation. Nucl. Tech. **41**(5), 050601 (2018). https://doi.org/10.11889/j.0253-3219.2018.hjs.41.050601. **(in Chinese)**
6. Q.Y. Li, B. Xu, C. Zhou et al., The optimization of flow rate distribution design of 373 MW molten salt reactor–liquid fuel. Nucl. Tech. **42**(7), 070605 (2019). https://doi.org/10.11889/j.0253-3219.2019.hjs.42.070605. **(in Chinese)**
7. C.W. Forsberg, The advanced high-temperature reactor: high-temperature fuel, liquid salt coolant, liquid–metal–reactor plant. Prog. Nucl. Energy **47**, 32–43 (2005)
8. S.R. Greene, J.C. Gehin, D.E. Holcomb et al., Pre-conceptual Design of a Fluoride-Salt-Cooled Small Modular Advanced High Temperature Reactor (SmAHTR). Technical Report TM-2010/199 (Oak Ridge National Laboratory, Tennessee, 2011). https://doi.org/10.2172/1008830

9. R. Yan, S.H. Yu, Y. Zou et al., Study on neutronics design of ordered-pebble-bed fluoride-salt-cooled high-temperature experimental reactor. Nucl. Sci. Tech. **29**, 81 (2018). https://doi.org/10.1007/s41365-018-0414-0
10. E. Shwageraus, H. Pavel, J.D. Michael, Liquid salt cooled flexible conversion ratio fast reactor: neutronic design. Nucl. Eng. Des. **239**(12), 2626–2645 (2009). https://doi.org/10.1016/j.nucengdes.2009.07.011
11. S.C. Zhou, L.Z. Cao, H.C. Wu et al., SPARK-LS: a novel design of a compact liquid chloride salt cooled fast reactor based on tube-in-duct fuel concept. Ann. Nucl. Energy **128**, 248–255 (2019). https://doi.org/10.1016/j.anucene.2019.01.020
12. J.A. Mascitti, M. Madariaga, Method for the calculation of DPA in the reactor pressure vessel of Atucha II. Sci. Technol. Nucl. Install. **2011**(12), 951–958 (2011). https://doi.org/10.1155/2011/534689
13. P. Mohanakrishnan, Physics Design of Core, IGCAR Design Report, PFBR/01113/DN/1049 (Rev.C) (Indira Gandhi Centre for Atomic Research, Kalpakkam, 2004)
14. T.A. Mehlhorn, B.B. Cipiti, C.L. Olson et al., Fusion-fission hybrids for nuclear waste transmutation: a synergistic step between Gen-IV fission and fusion reactors. Fusion Eng. Des. **83**(7–9), 948–953 (2008). https://doi.org/10.1016/j.fusengdes.2008.05.003
15. H.M. Şahin, Monte Carlo calculation of radiation damage in first wall of an experimental hybrid reactor. Ann. Nucl. Energy **34**(11), 861–870 (2007). https://doi.org/10.1016/j.anucene.2007.04.011
16. T.K. Kim, C. Grandy, R.N. Hill, Carbide and nitride fuels for advanced burner reactor. No. IAEA-CN–176 (POWERPOINT PRESENTATIONS) (2009)
17. C.R.F. Azevedo, Selection of fuel cladding material for nuclear fission reactors. Eng. Fail. Anal. **18**(8), 1943–1962 (2011). https://doi.org/10.1016/j.engfailanal.2011.06.010
18. M. Lin, M.S. Cheng, Z.M. Dai, Development and preliminary validation of a sub-channel analysis code for molten chloride-cooled fast reactor. Nucl. Tech. **42**, 010604 (2019). https://doi.org/10.11889/j.0253-3219.2019.hjs.42.010604. **(in Chinese)**
19. J.K. Zhang, R.J. McClure, P.R. Trapp et al., Lead–bismuth eutectic technology for hyperion reactor. J. Nucl. Mater. **441**(1), 644–649 (2013). https://doi.org/10.1016/j.jnucmat.2013.04.079
20. Y. Zhang, J. Wallenius, A. Fokau, Transmutation of americium in a medium size sodium cooled fast reactor design. Ann. Nucl. Energy **37**, 629–638 (2010). https://doi.org/10.1016/j.anucene.2009.12.014
21. R.C. Petroski, *Design of a 2400 MW Liquid-Salt Cooled Flexible Conversion Ratio Reactor* (Massachusetts Institute of Technology, Cambridge, 2008)
22. J. Sun, Q. Guo, Q.W. Zheng et al., Radiation response characteristics of an embeddable SOI radiation sensor. Nucl. Technol. **42**(12), 120501 (2019). https://doi.org/10.11889/j.0253-3219.2019.hjs.42.120501. **(in Chinese)**
23. D.F. Hollenbach, L.M. Petrie, N.F. Landers, KENO-VI: a general quadratic version of the KENO program. ORNL/TM-2005/39, Version 6
24. M.A. Jessee, M.D. DeHart, Triton: a multipurpose transport, depletion, and sensitivity and uncertainty analysis module. Oak Ridge National Laboratory, ORNL/TM-2005/39 Version 6 (2011)
25. B. Deng, J.G. Chen, L. He et al., Development and verification of a coupled code of steady-state neutronics and thermal-hydraulics for molten salt fast reactor. Nucl. Tech. **42**(11), 110602 (2019). https://doi.org/10.11889/j.0253-3219.2019.hjs.42.110602. **(in Chinese)**
26. M.S. Cheng, M. Lin, X.D. Zuo et al., Development and validation of a three-dimensional hexagonal nodal time-spatial kinetics code based on exponential transform. Nucl. Tech. **41**(6), 060604 (2018). https://doi.org/10.11889/j.0253-3219.2018.hjs.41.060604. **(in Chinese)**
27. http://www-nds.iaea.org/irdf2002/data/irdf2002damage.dat. Accessed June 2017
28. J. Chang, J. Cho, C. Gil et al., A simple method to calculate the displacement damage cross section of silicon carbide. Nucl. Eng. Technol. **46**(4), 475–480 (2014). https://doi.org/10.5516/NET.01.2013.051
29. B. Feng, K. Aydın, S.K. Mujid, Steady-state fuel behavior modeling of nitride fuels in FRAPCON-EP. J. Nucl. Mater. **427**(1–3), 30–38 (2012). https://doi.org/10.1016/j.jnucmat.2012.04.011
30. A.E. Waltar, R.T. Donald, V.T. Pavel, *Fast Spectrum Reactors* (Springer, Berlin, 2012)